

1 *Brief Communication*

2

3

4 **Deuteration provides a general strategy to enhance**
5 **azobenzene-based photopharmacology**

6
7 Kilian Roßmann^{1, #}, Alberto J. Gonzalez-Hernandez^{2, #}, Rahul Bhuyan³,
8 Karl Börjesson³, Joshua Levitz^{2,*}, Johannes Broichhagen^{1,*}

9
10 ¹ Leibniz-Forschungsinstitut für Molekulare Pharmakologie (FMP), 13125 Berlin, Germany.

11

12 ² Department of Biochemistry, Weill Cornell Medicine, New York, NY 10065, USA

13

14 ³ Department of Chemistry and Molecular Biology, University of Gothenburg, 413 90
15 Gothenburg, Sweden

16

17

18 [#] Equal contribution

19

20 * Correspondence should be addressed to:

21 jtl2003@med.cornell.edu and broichhagen@fmp-berlin.de

22

23 **ABSTRACT**

24 Herein, we present deuterated azobenzene photoswitches as a general means of enhancing
25 photopharmacological molecules. Deuteration can improve azobenzene performance in terms
26 of light sensitivity, photoswitch efficiency, and photoswitch kinetics with minimal alteration to
27 the underlying structure of the photopharmacological ligand. We report synthesized
28 deuterated azobenzene-based ligands for the optimized optical control of ion channel and G
29 protein-coupled receptor function in live cells, setting the stage for the straightforward,
30 widespread adoption of this approach.

31 **MAIN TEXT**

32 Photopharmacology represents a powerful means of optically controlling biological function
33 through the use of light-sensitive compounds^{1,2}. In addition to its use in a wide variety of basic
34 science applications³⁻¹², photopharmacology has now entered clinical trials via KIO-301, a
35 photoswitchable ion channel blocker with great potential for vision restoration¹³. This
36 compound utilizes an azobenzene-based photoswitch, which represents one of the primary
37 chemical moieties used in photopharmacological probes¹⁴. Despite their many advantageous
38 properties¹⁵, azobenzene photoswitch performance is typically limited by light sensitivity,
39 photoisomerization efficiency, and photoswitching speed which together reduce their ability to
40 enable robust and rapid light-dependent control in complex biological systems. In recent years,
41 multiple strategies have emerged to improve the properties of azobenzene-based
42 photoswitches. Most typical has been derivatization of the azobenzene itself which can
43 enhance critical photophysical properties (extinction coefficient, wavelength tuning, bistability
44 etc.) by a diverse array of chemical modifications, introducing heterocycles or halogen atoms
45 on the aromatic units, creating push-pull systems or the installment of sensitive “antennas” for
46 2-photon activation^{14,16-25}. To enable improved target selectivity and genetic precision,
47 covalent tethering to cysteines or self-labelling enzymes (e.g. SNAP-tag) has also been used.
48 We recently reported a strategy to effectively improve tethered photopharmacology efficiency
49 by branching multiple azobenzene switches onto the same molecule^{26,27}.

50 Despite their utility, all of the aforementioned techniques involve chemical modifications to the
51 underlying compound, thus altering the core structure of the molecule. This makes the process
52 of improving photopharmacological ligands laborious and molecule-specific and raises the
53 possibility that chemical modifications will not be tolerated due to constraints of the target
54 molecule’s binding site. Methods that can be broadly applied to any azobenzene-based
55 system without the need for compound-specific engineering are, thus, needed. One such
56 option is to pursue deuteration, which introduces isotope effects without altering the structure
57 of the chromophore itself. Motivated by recent studies showing that installation of deuterium

58 can enhance fluorophore performance²⁸⁻³⁰ (**Figure 1A**), we asked if similar improvements may
59 be obtained with azobenzene photoswitch chromophores (**Figure 1B**). Deuterated
60 azobenzenes have been described before to investigate drug metabolism³¹, to study ¹³C shifts
61 in NMR spectroscopy³², or to obtain “IR clean” switches³³. However, to our knowledge, no
62 reports exist that explore deuterated azobenzenes in photopharmacological settings.

63 We first aimed for the simplest model system, a ‘naked’ azobenzene with either 10 hydrogens
64 (“AB-h10”) or 10 deuteriums (“AB-d10”) (**Figure 1B**, R = D). Synthesis was straightforwardly
65 achieved from non-deuterated or deuterated nitrobenzene using zinc as a reducing agent in
66 refluxing methanol, and the desired azobenzenes were obtained in 51% and 45% yields,
67 respectively (**Figure 1C**). We characterized the photophysical properties of these molecules
68 and found that the maximal absorbance wavelength in DMSO remained unchanged at 322
69 nm (**Figure 1D**). Since no hydrogen atoms are present in azobenzene-d10, we next performed
70 hydrogen-coupled, quantitative ¹³C NMR to determine concentrations using DMF as an
71 internal standard, and found using UV/Vis spectroscopy that extinction coefficient was
72 increased by >50% ($\epsilon_{322 \text{ nm}} = 20,800$ versus $32,000 \text{ M}^{-1} \text{ cm}^{-1}$) for AB-d10 (**Figure 1D**).
73 Impressed by this change, and to exclude distortions by nuclear Overhauser effects due to
74 different nuclei, we confirmed this trend by weighing each compound and observed the
75 extinction coefficient to be increased by ~20% due to deuteration ($\epsilon_{322 \text{ nm}} = 17,800$ versus
76 $21,300 \text{ M}^{-1} \text{ cm}^{-1}$) (**Figure 1D**). We note that in both cases, AB-h10 was close to reported
77 literature values of $22,400 \text{ M}^{-1} \text{ cm}^{-1}$ at 319 nm in methanol.³⁴ Interestingly, by plotting the
78 absorbance of the deuterated divided by the absorbance of the non-deuterated azobenzene,
79 we observed a subtle change in spectra around the maximal absorbance peak (**Figure 1E**),
80 indicating different vibrational states for the two molecules. To further examine this, we
81 recorded IR spectra of AB-h10 and AB-d10 and found, as expected, differences in the
82 fingerprint region (**Figure 1F**). Most relevant to potential photopharmacological applications,
83 we also observed a clear acceleration in *trans*-to-*cis* ($\tau = 6.61$ vs. 6.27 sec) and *cis*-to-*trans*
84 ($\tau = 1.47$ vs. 1.39 sec) photoswitching kinetics for azobenzene-d10 in DMSO (**Figure 1G**).

85 Encouraged by the above results indicating that deuteration can improve azobenzenes, we
86 pursued a water soluble azobenzene-based compound since organic solvent effects do not
87 recapitulate the cellular environment where most photoswitches are, ultimately, applied. We
88 chose azobenzene quaternary ammonium (AQ) as a scaffold as it is bis-amidated and, thus,
89 carries a charge for excellent water solubility. AQ has been used with various substituents to
90 optically control potassium channels in a plethora of studies on nociception, vision restoration,
91 and neuromodulation (**Figure 2A**)^{13,23,35-39}. We synthesized deuterated AQ-d8 by oxidatively
92 dimerizing phenylene diamine-d4 (**1**) with Dess-Martin periodinane to obtain a perdeuterated

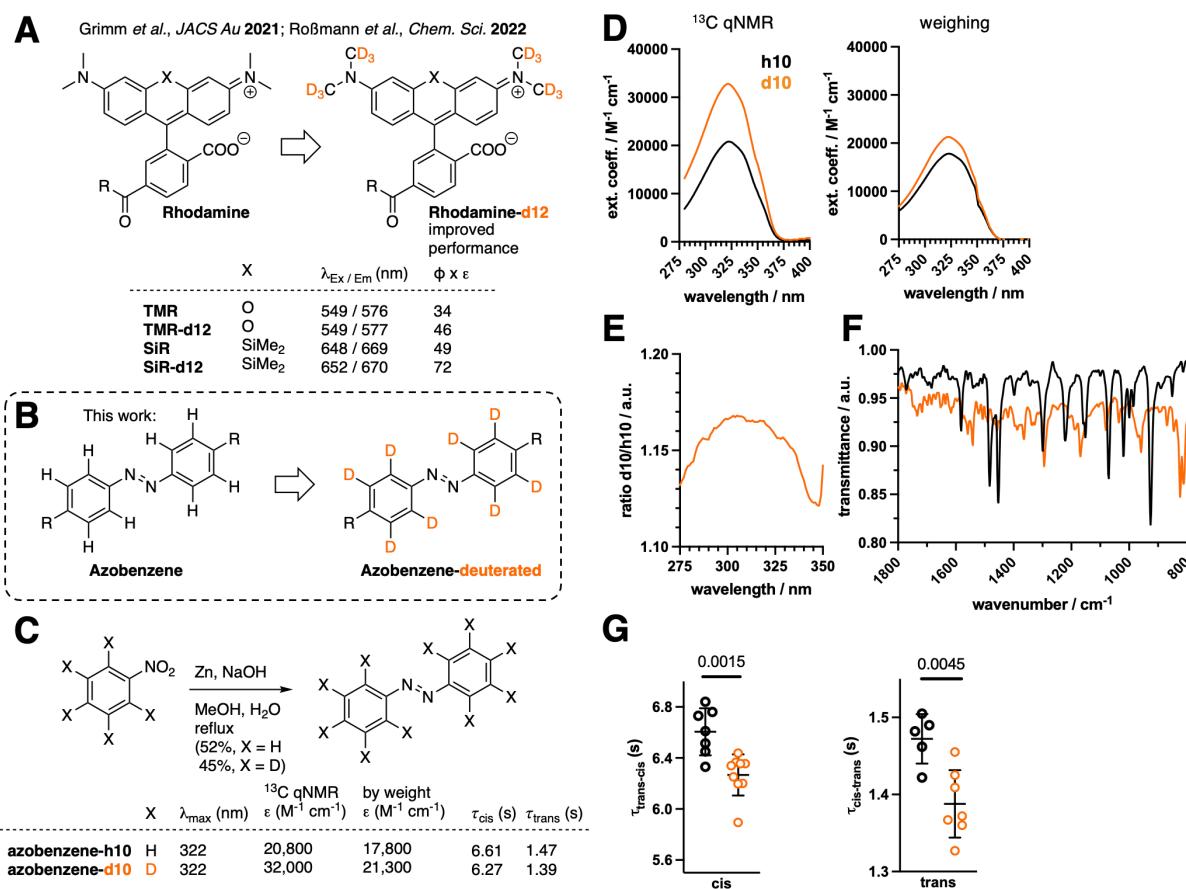
93 4,4'-bisamine azobenzene **2**, before HBTU-mediated coupling to betaine and subsequent
94 acylation using acetyl chloride (**Figure 2B**). We profiled AQ-h8 and AQ-d8 and found relatively
95 unchanged maximal absorbance at 363 nm and 360 nm (**Figure 2C**), respectively. We
96 determined extinction coefficients in water to be $15,200 \text{ M}^{-1} \text{ cm}^{-1}$ for both compounds via ^1H
97 qNMR using DMF as an internal standard (**Figure 2C**). We probed the change in UV/Vis
98 absorbance by looking at the ratio of values for AQ-h8 and AQ-d8 and found subtle changes
99 around the maximal absorbance value (**Figure 2D**). IR spectra also showed distinct shifts in
100 vibrational motions (**Figure 2E**), indicating differences due to the deuterium isotopes. ^1H
101 qNMR measurements allowed us to determine photostationary states (as described
102 previously²³) in D_2O under 385 nm, 500 nm and 525 nm irradiation where similar values were
103 seen for both compounds (**Figure 2F**). We also determined quantum yields for *trans*-to-*cis*
104 switching and found these to be similar ($\Phi(\text{AQ-h8}) = 32\%$; $\Phi(\text{AQ-d8}) = 31\%$)⁴⁰. While such
105 modest differences would likely not strongly influence performance in a photopharmacological
106 setting, we observed that switching kinetics were much faster for AQ-d8 than AQ-h8 (*trans*-to-
107 *cis*: $\tau = 9.91$ vs. 5.42 sec; *cis*-to-*trans*: $\tau = 6.11$ vs. 4.18 sec) (**Figure 2G**). Encouraged by this,
108 we tested the ability of AQ-h8 and AQ-d8 to control the activity of large conductance voltage
109 and calcium-gated (BK) potassium channels *via* patch-clamp electrophysiology in HEK 293
110 cells. We delivered 1 mM of AQ-h8 or AQ-d8 to the cytosol *via* the patch pipette and observed
111 robust, reversible photo-block and photo-unblock by illuminating successively with 525 nm
112 and 385 nm light (**Figure 2H**). While the efficiency of photoblock was similar for AQ-h8 and
113 AQ-d8 (**Figure S1A, B**), AQ-d8 showed substantially faster photoswitch kinetics (**Figure 2I**).
114 Importantly, given that AQ acts as a simple pore blocker, photocurrent kinetics likely serve as
115 a direct readout of *cis/trans* switching kinetics.

116 Photopharmacology can be merged with the power of genetic engineering by tethering
117 photoswitchable ligands to a self-labelling tag (e.g. SNAP) on a protein of interest²⁶. This
118 approach yields excellent target selectivity due to the biorthogonal nature of labelling and rapid
119 photoswitching kinetics due to the lack of ligand diffusion. We pioneered this approach by
120 conjugating the SNAP-tagged metabotropic glutamate receptor 2 (SNAP-mGluR2), a
121 neuromodulatory GPCR, with a “photoswitchable orthogonal remotely-tethered ligand”
122 (PORTL) which enables rapid, reversible optical control of mGluR2 activity *ex vivo* and *in vivo*
123 (**Figure 3A**)^{23,27,41}. The PORTL ligand consists of a benzylguanine-azobenzene-glutamate
124 (“BGAG”) photoswitch, with BGAG₁₂-v2-h8 serving as a testbed for our deuteration strategy.
125 Employing a previously described synthetic route (**Figure 3B; Supplementary Information**),
126 we obtained deuterated BGAG₁₂-v2-d8, which showed the same maximal absorbance
127 wavelength of BGAG₁₂-v2-h8 (**Figure 3B; Figure S2A**). BGAG₁₂-v2-d8 labelled SNAP-
128 mGluR2 transfected HEK293 cells with the same efficiency as its non-deuterated counterpart

129 **(Figure S2B, C).** Using patch-clamp electrophysiology with G protein-coupled inward-
130 rectifying potassium (GIRK) channels as a reporter, we observed robust and reversible
131 responses by applying 385 nm (ON) and 525 nm (OFF) light (**Figure 3C**). When comparing
132 photocurrents to the response to a saturating concentration of glutamate (1 mM), a clear
133 increase in photoswitching efficiency was observed from ~50% to ~68% for BGAG₁₂-v2-d8
134 (**Figure 3D**). In addition, we observed a faster ON response when 385 nm light was applied
135 (**Figure 3E**). It should be noted that OFF kinetics, which do not change between BGAG₁₂-v2-
136 d8 and BGAG₁₂-v2, do not recapitulate photoswitch kinetics in this system but are limited by
137 biological signal termination processes. Nevertheless, the PORTL system allows for a clean
138 readout since photoswitch concentration is determined by receptor expression level.

139 In summary, we have translated the deuteration strategy from fluorophores to azobenzene
140 photoswitches, where we find substantially improved properties. Future work is needed to fully
141 decipher the underlying photophysical mechanism. We demonstrate the ability of deuteration
142 to enhance azobenzene photoswitching on two distinct systems, a soluble photochromic
143 ligand (AQ) and a tethered PORTL (BGAG), suggesting that this strategy can be widely
144 applicable to the many azobenzene scaffolds and ligands which have been reported as
145 photopharmacological tools. Interestingly, while all three compounds reported here showed
146 clearly improved photoswitch kinetics, there was variability in the extent of effects on light
147 absorbance and photoswitch efficiency, motivating future analyses of the vast chemical space
148 for deuteration (or semi-deuteration) on the aromatic units of an azobenzene and/or their
149 substituents (e.g. *N*-methyl amine deuteration) to further optimize this strategy.

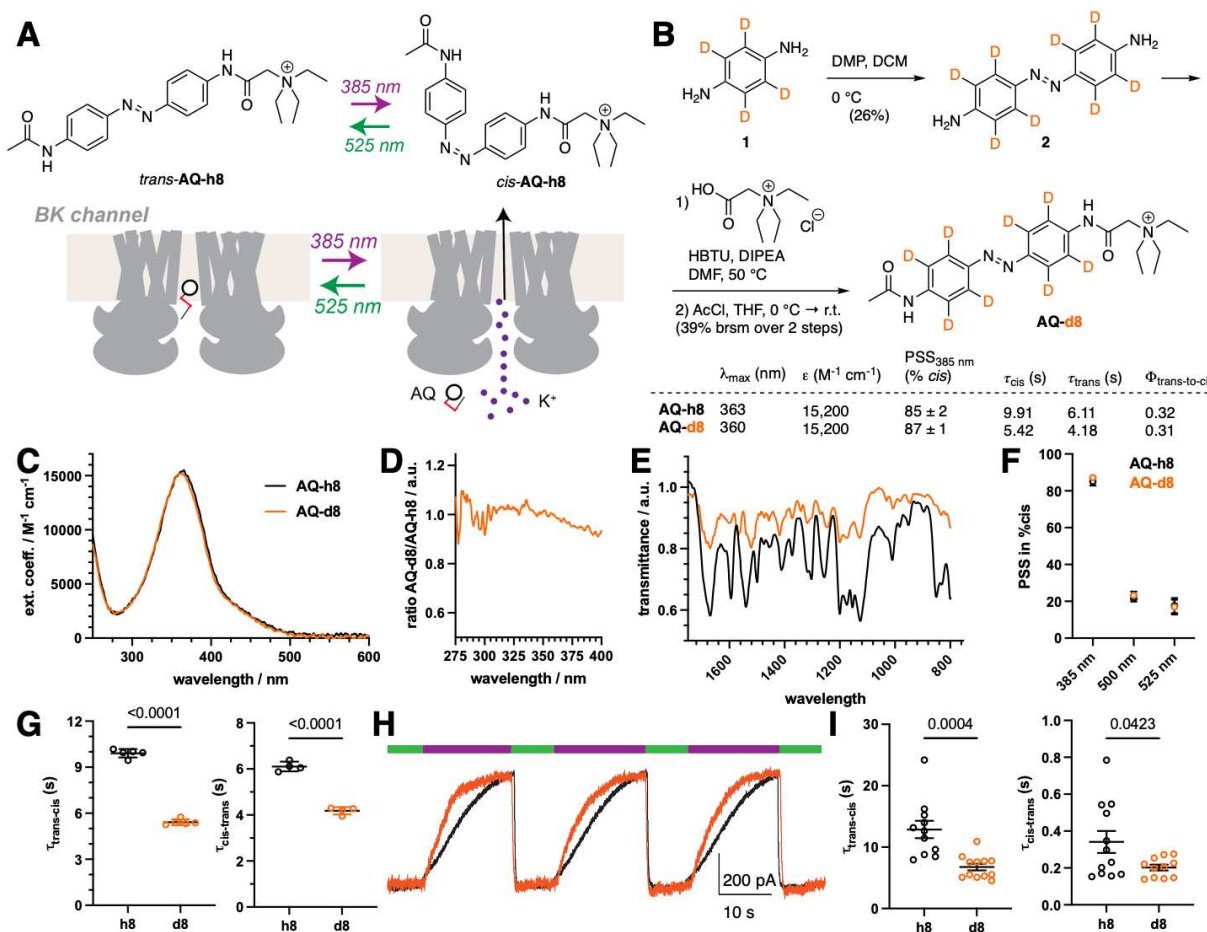
150 **FIGURES**



151

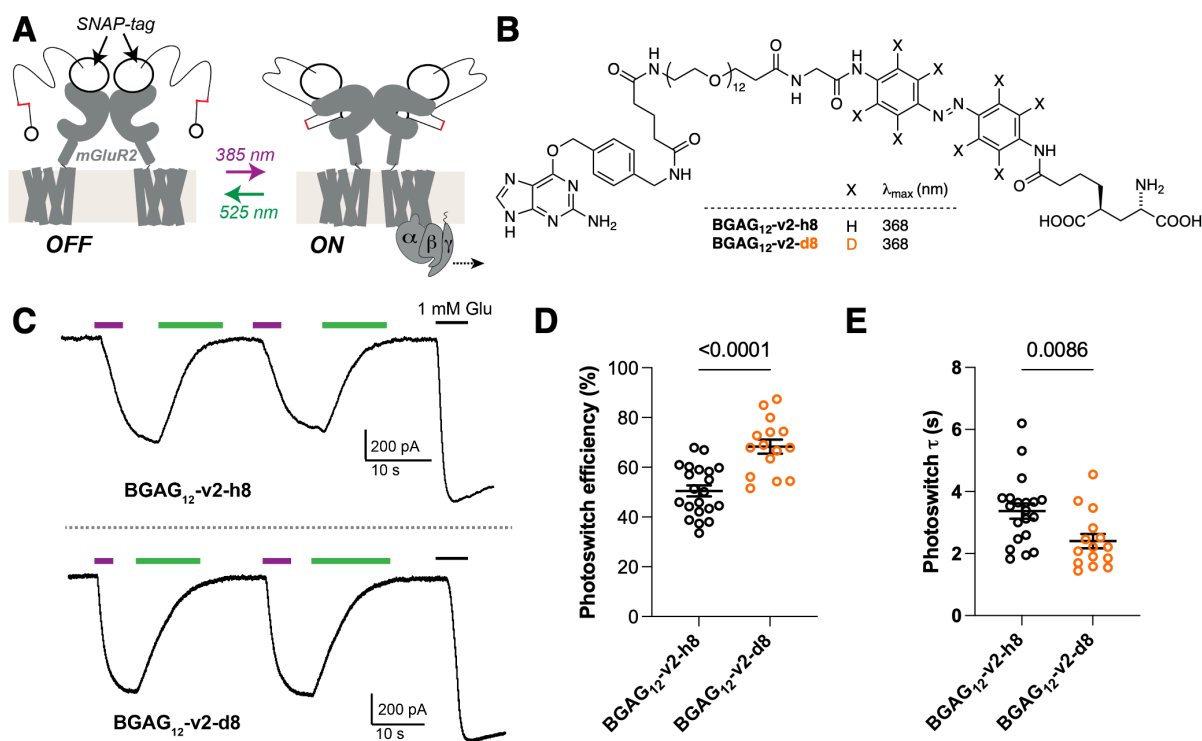
152 **Figure 1: Deuteration strategy to enhance photophysical properties.** **A)** Enhanced
153 fluorophore performance was previously obtained by installing deuterated *N*-methyl
154 rhodamines. While excitation/emission spectra show minute changes, brightness ($\Phi \times \epsilon$) is
155 drastically enhanced by deuteration. **B)** In this work, we extend this concept by perdeutering
156 azobenzene chromophores. **C)** Synthesis of azobenzene-d10 by reductive dimerization of
157 nitrobenzene using zinc. Extinction coefficient and switching kinetics are increased by
158 deuteration. **D-E)** UV/Vis spectra and extinction coefficient determination of azobenzene-h10
159 and azobenzene-d10 in DMSO by ^{13}C qNMR (left) or by weighing (right). **E)** Ratio of
160 azobenzene-d10 and azobenzene-h10 shows different absorbance characteristics. **F)** IR
161 spectra of azobenzene-d10 and azobenzene-h10 shows distinct vibrational states. **G)**
162 Switching kinetics for trans-to-cis (left) and cis-to-trans (right) photoconversion of azobenzene-
163 h10 and azobenzene-d10 in DMSO. P-values from unpaired t-tests are reported in panel G.

164



165

Figure 2: Deuteration enhances performance of a soluble, photoswitchable potassium channel blocker. A) *trans*-AQ blocks potassium channels at an intracellular site and unblocking can be achieved optically by applying 385 nm light, with reversibility using 525 nm light. **B)** Synthesis of AQ-d8 and summary of photophysical properties. **C)** UV/Vis spectra and extinction coefficient determination of AQ-h8 and AQ-d8 in water by ¹H qNMR. **D)** Ratio of AQ-h8 and AQ-d8 shows different absorbance characteristics. **E)** IR spectra of AQ-h8 and AQ-d8 shows different vibrational states. **F)** Photostationary state occupancies under different wavelengths as assessed by ¹H qNMR. **G)** *in vitro* Switching kinetics of AQ-h8 and AQ-d8. **H)** BK channel representative trace at +60 mV in response to 385 nm (purple) and 525 nm (green) light in the presence of AQ-h8 or AQ-d8. **I)** Quantification of channel photo-unblock (left) and photo-block (right) kinetics. P-values from unpaired t-tests are reported in panels G and I.



178 **Figure 3: Deuteration enables more efficient, faster optical control of a GPCR via a**
179 **tethered photoswitch. A)** Schematic showing optical control of mGluR2-mediated G protein
180 signalling via the PORTL “BGAG”. BGAG is attached to an N-terminal fused SNAP-tag and
181 activates mGluR2 upon 385 nm light and can be turned off using 525 nm light. **B)** Structure of
182 BGAG₁₂-v2-h8/d8. **C-E)** GIRK current recordings of SNAP-mGluR2 photoswitching reveals
183 reversibility and repeatability of switching, and increased performance of BGAG₁₂-v2-d8 in
184 terms of efficiency (D) and kinetics (E). P-values from unpaired t-tests reported in panels D
185 and E.

186 **MATERIALS and METHODS**

187 **Chemical synthesis**

188 Chemical synthesis and characterization procedures are reported in the Supporting
189 Information.

190 **Cell culture, molecular biology and patch clamp electrophysiology**

191 HEK293 cells were cultured in Dulbecco's Modified Eagle Medium (DMEM; Corning)
192 supplemented with 10% fetal bovine serum (FBS) and maintained at 37° C and 5% CO₂. Cells
193 were seeded at low density in poly-L-lysine coated 18 mm coverslips and transfected the
194 following day with Lipofectamine 2000 (Thermo Fisher Scientific). Plasmid expressing BK
195 channel human alpha subunit (pBNJ13-hSlo)⁴² was kindly gifted by Prof. Teresa Giraldez
196 (University of La Laguna, Spain). This construct was used for testing AQ compounds. For
197 BGAG recordings, SNAP-mGluR2⁴³, GIRK1-F137S⁴⁴ and tdTomato as a transfection marker
198 were co-transfected in cells in a 1:1:0.2 ratio.

199 Whole cell patch clamp recordings were performed 24 hr after transfection using an
200 Axopatch 200B amplifier and a Digidata 1550B interface controlled by pClampex software
201 (Molecular Devices). Recordings were performed in a bath solution containing (in mM): 120
202 KCl, 25 NaCl, 10 HEPES, 2 CaCl₂, 1 MgCl₂. Pipettes of 3-5 MΩ resistance were filled with
203 intracellular solution (in mM: 140 KCl, 10 HEPES, 5 EGTA, 3 MgCl₂, 3 Na₂ATP, 0.2 Na₂GTP).
204 For AQ compounds, AQ-h8 and AQ-d8 were added to a final concentration of 1 mM in the
205 pipette solution. For BGAG, cells were labelled with 1 μM of BGAG₁₂-v2-h8 or BGAG₁₂-v2-d8
206 for 45 min at 37°C in extracellular solution. Labeling efficiency was measured using a
207 fluorophore competition assay as previously.⁴⁵ Photoactivation of the compounds was
208 obtained through a computer controlled CoolLED pE-4000 attached to an inverted microscope
209 and through a 40x objective. Light intensities at the focal plane were (in mW/mm²): 5.6 for 385
210 nm and 4.9 for 525 nm. For AQ compound photoswitching, a 0.1% neutral density ND filter
211 (Chroma) was added to the 385 nm illumination path to produce lower light conditions for
212 kinetics analysis (5.57 μW/mm²).

213 To obtain an I-V curve for BK channel activation, a step protocol of 50 ms of pulse
214 ranging from -100 mV to + 200 mV in +20 mV increments was recorded. This was done in the
215 presence of either wavelength (385 nm or 525 nm) throughout each sweep. Steady-state
216 current at the end of the pulse, normalized to the maximum current observed in each individual
217 cell, was plotted against the voltage applied to each step. The protocol for photoswitching of
218 AQ compounds consisted of a voltage clamp of the cell at + 60 mV and applying pulses of 20
219 s of 385 nm immediately followed by 10 s of 525 nm light. For BGAG recordings,
220 photoactivation by 385 nm was performed until the mGluR2 evoked GIRK current was in a

221 steady state and after that, was quickly switched off by 525 nm light. Photoswitch efficiency
222 was calculated as the amplitude of the 385 nm evoked current divided by the amplitude of the
223 current response to saturating 1 mM glutamate.

224 All cellular data comes from at least three separate transfections/experimental days.
225 Data was analyzed using Clampfit (Molecular Devices) and Prism 9 (GraphPad). AQ and
226 BGAG trans-to-cis kinetics were quantified by fitting the evoked currents to a single
227 exponential.

228 **ACKNOWLEDGEMENTS**

229 This project has received funding from the European Union's Horizon Europe Framework
230 Programme (deuterON, grant agreement no. 101042046 to JB). A.G-H. is funded by the
231 Margarita Salas Fellowship from the Spanish Ministry of Universities. J.L. is supported by the
232 Rohr Family Research Scholar Award and the Irma T. Hirsch and Monique Weill-Caulier
233 Award. We thank Aditi Jain for technical assistance.

234 **COMPETING INTERESTS**

235 The authors declare no competing interests.

236 **REFERENCES**

- 237 1. Kobauri, P., Dekker, F.J., Szymanski, W., and Feringa, B.L. (2023). Rational Design in
238 Photopharmacology with Molecular Photoswitches. *Angew Chem Int Ed* 62, e202300681.
239 10.1002/anie.202300681.
- 240 2. Hüll, K., Morstein, J., and Trauner, D. (2018). *In Vivo Photopharmacology*. *Chem. Rev.*
241 118, 10710–10747. 10.1021/acs.chemrev.8b00037.
- 242 3. Borowiak, M., Küllmer, F., Gegenfurtner, F., Peil, S., Nasufovic, V., Zahler, S., Thorn-
243 Seshold, O., Trauner, D., and Arndt, H.-D. (2020). Optical Manipulation of F-Actin with
244 Photoswitchable Small Molecules. *J. Am. Chem. Soc.* 142, 9240–9249.
245 10.1021/jacs.9b12898.
- 246 4. Kolarski, D., Miró-Vinyals, C., Sugiyama, A., Srivastava, A., Ono, D., Nagai, Y., Iida, M.,
247 Itami, K., Tama, F., Szymanski, W., et al. (2021). Reversible modulation of circadian time
248 with chronopharmacology. *Nat Commun* 12, 3164. 10.1038/s41467-021-23301-x.
- 249 5. Zhou, H., Xue, C., Weis, P., Suzuki, Y., Huang, S., Koynov, K., Auernhammer, G.K.,
250 Berger, R., Butt, H.-J., and Wu, S. (2017). Photoswitching of glass transition temperatures
251 of azobenzene-containing polymers induces reversible solid-to-liquid transitions. *Nature
252 Chem* 9, 145–151. 10.1038/nchem.2625.
- 253 6. Ma, X., Johnson, D.A., He, X.J., Layden, A.E., McClain, S.P., Yung, J.C., Rizzo, A.,
254 Bonaventura, J., and Banghart, M.R. (2023). In vivo photopharmacology with a caged mu
255 opioid receptor agonist drives rapid changes in behavior. *Nat Methods* 20, 682–685.
256 10.1038/s41592-023-01819-w.

257 7. Kainrath, S., Stadler, M., Reichhart, E., Distel, M., and Janovjak, H. (2017). Green-Light-
258 Induced Inactivation of Receptor Signaling Using Cobalamin-Binding Domains. *Angew*
259 *Chem Int Ed* 56, 4608–4611. 10.1002/anie.201611998.

260 8. Sarott, R.C., Viray, A.E.G., Pfaff, P., Sadybekov, A., Rajic, G., Katritch, V., Carreira, E.M.,
261 and Frank, J.A. (2021). Optical Control of Cannabinoid Receptor 2-Mediated Ca^{2+}
262 Release Enabled by Synthesis of Photoswitchable Probes. *J. Am. Chem. Soc.* 143, 736–
263 743. 10.1021/jacs.0c08926.

264 9. Pereira, V., Arias, J.A., Llebaria, A., and Goudet, C. (2023). Photopharmacological
265 manipulation of amygdala metabotropic glutamate receptor mGlu4 alleviates neuropathic
266 pain. *Pharmacological Research* 187, 106602. 10.1016/j.phrs.2022.106602.

267 10. Izquierdo-Serra, M., Bautista-Barrufet, A., Trapero, A., Garrido-Charles, A., Díaz-
268 Tahoces, A., Camarero, N., Pittolo, S., Valbuena, S., Pérez-Jiménez, A., Gay, M., et al.
269 (2016). Optical control of endogenous receptors and cellular excitability using targeted
270 covalent photoswitches. *Nature Communications* 7, 12221. 10.1038/ncomms12221.

271 11. Thapaliya, E.R., Mony, L., Sanchez, R., Serraz, B., Paoletti, P., and Ellis-Davies, G.C.R.
272 (2021). Photochemical Control of Drug Efficacy: A Comparison of Uncaging and
273 Photoswitching Ifenprodil on NMDA Receptors. *ChemPhotoChem* 5, 445–454.
274 10.1002/cptc.202000240.

275 12. Duffet, L., Tatarskiy, P.V., Harada, M., Williams, E.T., Hartrampf, N., and Patriarchi, T.
276 (2022). A photocaged orexin-B for spatiotemporally precise control of orexin signaling.
277 *Cell Chemical Biology* 29, 1729–1738.e8. 10.1016/j.chembiol.2022.11.007.

278 13. Daniels, E., Barras, C., Dwyer, A., Strem, B., Wykoff, C.C., Van Gelder, R.N., and
279 Casson, R.J. (2023). An Intravitreal “Photoswitch” Molecule (KIO-301) for Reanimation in
280 Retinitis Pigmentosa: a first-in-human trial. *Investigative Ophthalmology & Visual Science*
281 64, 5444–5444.

282 14. Jerca, F.A., Jerca, V.V., and Hoogenboom, R. (2021). Advances and opportunities in the
283 exciting world of azobenzenes. *Nat Rev Chem* 6, 51–69. 10.1038/s41570-021-00334-w.

284 15. Beharry, A.A., and Woolley, G.A. (2011). Azobenzene photoswitches for biomolecules.
285 *Chem. Soc. Rev.* 40, 4422. 10.1039/c1cs15023e.

286 16. Weston, C.E., Richardson, R.D., Haycock, P.R., White, A.J.P., and Fuchter, M.J. (2014).
287 Arylazopyrazoles: Azoheteroarene Photoswitches Offering Quantitative Isomerization and
288 Long Thermal Half-Lives. *J. Am. Chem. Soc.* 136, 11878–11881. 10.1021/ja505444d.

289 17. Bléger, D., Schwarz, J., Brouwer, A.M., and Hecht, S. (2012). o-Fluoroazobenzenes as
290 Readily Synthesized Photoswitches Offering Nearly Quantitative Two-Way Isomerization
291 with Visible Light. *J. Am. Chem. Soc.* 134, 20597–20600. 10.1021/ja310323y.

292 18. Broichhagen, J., Frank, J.A., Johnston, N.R., Mitchell, R.K., Smid, K., Marchetti, P.,
293 Bugliani, M., Rutter, G.A., Trauner, D., and Hodson, D.J. (2015). A red-shifted
294 photochromic sulfonylurea for the remote control of pancreatic beta cell function. *Chem.*
295 *Commun.* 51, 6018–6021. 10.1039/c5cc01224d.

296 19. Konrad, D.B., Frank, J.A., and Trauner, D. (2016). Synthesis of Redshifted Azobenzene
297 Photoswitches by Late-Stage Functionalization. *Chemistry – A European Journal* 22,
298 4364–4368. 10.1002/chem.201505061.

299 20. Konrad, D.B., Savasci, G., Allmendinger, L., Trauner, D., Ochsenfeld, C., and Ali, A.M.
300 (2020). Computational Design and Synthesis of a Deeply Red-Shifted and Bistable
301 Azobenzene. *J. Am. Chem. Soc.* **142**, 6538–6547. 10.1021/jacs.9b10430.

302 21. Siewertsen, R., Neumann, H., Buchheim-Stehn, B., Herges, R., Näther, C., Renth, F.,
303 and Temps, F. (2009). Highly Efficient Reversible *Z-E* Photoisomerization of a Bridged
304 Azobenzene with Visible Light through Resolved S_1 ($n\pi^*$) Absorption Bands. *J. Am.*
305 *Chem. Soc.* **131**, 15594–15595. 10.1021/ja906547d.

306 22. Samanta, S., Beharry, A.A., Sadovski, O., McCormick, T.M., Babalhavaeji, A., Tropepe,
307 V., and Woolley, G.A. (2013). Photoswitching Azo Compounds *in Vivo* with Red Light. *J.*
308 *Am. Chem. Soc.* **135**, 9777–9784. 10.1021/ja402220t.

309 23. Gutzeit, V.A., Acosta-Ruiz, A., Munguba, H., Häfner, S., Landra-Willm, A., Mathes, B.,
310 Mony, J., Yarotski, D., Börjesson, K., Liston, C., et al. (2021). A fine-tuned azobenzene for
311 enhanced photopharmacology *in vivo*. *Cell Chemical Biology* **28**, 1648–1663.e16.
312 10.1016/j.chembiol.2021.02.020.

313 24. Pfaff, P., Anderl, F., Fink, M., Balkenhohl, M., and Carreira, E.M. (2021). Azoacetylenes
314 for the Synthesis of Arylazotriazole Photoswitches. *J. Am. Chem. Soc.* **143**, 14495–14501.
315 10.1021/jacs.1c06014.

316 25. Cabré, G., Garrido-Charles, A., Moreno, M., Bosch, M., Porta-de-la-Riva, M., Krieg, M.,
317 Gascón-Moya, M., Camarero, N., Gelabert, R., Lluch, J.M., et al. (2019). Rationally
318 designed azobenzene photoswitches for efficient two-photon neuronal excitation. *Nat*
319 *Commun* **10**, 907. 10.1038/s41467-019-08796-9.

320 26. Broichhagen, J., and Levitz, J. (2022). Advances in tethered photopharmacology for
321 precise optical control of signaling proteins. *Current Opinion in Pharmacology* **63**, 102196.
322 10.1016/j.coph.2022.102196.

323 27. Acosta-Ruiz, A., Gutzeit, V.A., Skelly, M.J., Meadows, S., Lee, J., Parekh, P., Orr, A.G.,
324 Liston, C., Pleil, K.E., Broichhagen, J., et al. (2020). Branched Photoswitchable Tethered
325 Ligands Enable Ultra-efficient Optical Control and Detection of G Protein-Coupled
326 Receptors *In Vivo*. *Neuron* **105**, 446–463.e13. 10.1016/j.neuron.2019.10.036.

327 28. Grimm, J.B., Xie, L., Casler, J.C., Patel, R., Tkachuk, A.N., Falco, N., Choi, H.,
328 Lippincott-Schwartz, J., Brown, T.A., Glick, B.S., et al. (2021). A General Method to
329 Improve Fluorophores Using Deuterated Auxochromes. *JACS Au* **1**, 690–696.
330 10.1021/jacsau.1c00006.

331 29. Roßmann, K., Akkaya, K.C., Poc, P., Charbonnier, C., Eichhorst, J., Gonschior, H.,
332 Valavalkar, A., Wendler, N., Cordes, T., Dietzek-Ivanšić, B., et al. (2022). *N*-Methyl
333 deuterated rhodamines for protein labelling in sensitive fluorescence microscopy. *Chem.*
334 *Sci.* **13**, 8605–8617. 10.1039/D1SC06466E.

335 30. Janeková, H., Friedman, H.C., Russo, M., Ahmed, T., Zyberaj, M., Hua, S., Sica, A.V.,
336 Caram, J.R., and Stacko, P. (2023). Deuteration of Heptamethine Cyanine Dyes Leads to
337 Enhanced Emission Efficacy (Chemistry) 10.26434/chemrxiv-2023-c81hj.

338 31. Mori, Y., Niwa, T., and Toyoshi, K. (1981). Syntheses of Deuterated 3'-Hydroxymethyl-4-
339 (dimethylamino)-azobenzene and Related Compound. *RADIOISOTOPES* **30**, 86–91.
340 10.3769/radioisotopes.30.2_86.

341 32. Vikić-Topić, D., Novak, P., Smrečki, V., and Meić, Z. (1997). Deuterium isotope effects in
342 ¹³C NMR spectra of trans-azobenzene. *Journal of Molecular Structure* 410–411, 5–7.
343 10.1016/S0022-2860(96)09665-2.

344 33. Pfister, R., Ihlainen, J., Hamm, P., and Kolano, C. (2008). Synthesis, characterization
345 and applicability of three isotope labeled azobenzene photoswitches. *Org. Biomol. Chem.*
346 6, 3508. 10.1039/b804568b.

347 34. Zimmerman, G., Chow, L.-Y., and Paik, U.-J. (1958). The Photochemical Isomerization of
348 Azobenzene¹. *J. Am. Chem. Soc.* 80, 3528–3531. 10.1021/ja01547a010.

349 35. Banghart, M.R., Mourot, A., Fortin, D.L., Yao, J.Z., Kramer, R.H., and Trauner, D. (2009).
350 Photochromic blockers of voltage-gated potassium channels. *Angew. Chem. Int. Ed. Engl.*
351 48, 9097–9101. 10.1002/anie.200904504.

352 36. Mourot, A., Fehrentz, T., Le Feuvre, Y., Smith, C.M., Herold, C., Dalkara, D., Nagy, F.,
353 Trauner, D., and Kramer, R.H. (2012). Rapid optical control of nociception with an ion-
354 channel photoswitch. *Nat. Methods* 9, 396–402. 10.1038/nmeth.1897.

355 37. Fortin, D.L., Banghart, M.R., Dunn, T.W., Borges, K., Wagenaar, D.A., Gaudry, Q.,
356 Karakossian, M.H., Otis, T.S., Kristan, W.B., Trauner, D., et al. (2008). Photochemical
357 control of endogenous ion channels and cellular excitability. *Nat Methods* 5, 331–338.
358 10.1038/nmeth.1187.

359 38. Tochitsky, I., Polosukhina, A., Degtyar, V.E., Gallerani, N., Smith, C.M., Friedman, A.,
360 Van Gelder, R.N., Trauner, D., Kaufer, D., and Kramer, R.H. (2014). Restoring Visual
361 Function to Blind Mice with a Photoswitch that Exploits Electrophysiological Remodeling
362 of Retinal Ganglion Cells. *Neuron* 81, 800–813. 10.1016/j.neuron.2014.01.003.

363 39. Sandoz, G., Levitz, J., Kramer, R.H., and Isacoff, E.Y. (2012). Optical Control of
364 Endogenous Proteins with a Photoswitchable Conditional Subunit Reveals a Role for
365 TREK1 in GABAB Signaling. *Neuron* 74, 1005–1014. 10.1016/j.neuron.2012.04.026.

366 40. Stranius, K., and Börjesson, K. (2017). Determining the Photoisomerization Quantum
367 Yield of Photoswitchable Molecules in Solution and in the Solid State. *Sci Rep* 7, 41145.
368 10.1038/srep41145.

369 41. Broichhagen, J., Damijonaitis, A., Levitz, J., Sokol, K.R., Leippe, P., Konrad, D., Isacoff,
370 E.Y., and Trauner, D. (2015). Orthogonal Optical Control of a G Protein-Coupled Receptor
371 with a SNAP-Tethered Photochromic Ligand. *ACS Cent. Sci.* 1, 383–393.
372 10.1021/acscentsci.5b00260.

373 42. Giraldez, T., Hughes, T.E., and Sigworth, F.J. (2005). Generation of Functional
374 Fluorescent BK Channels by Random Insertion of GFP Variants. *The Journal of General
375 Physiology* 126, 429–438. 10.1085/jgp.200509368.

376 43. Doumazane, E., Scholler, P., Zwier, J.M., Trinquet, E., Rondard, P., and Pin, J.P. (2011).
377 A new approach to analyze cell surface protein complexes reveals specific heterodimeric
378 metabotropic glutamate receptors. *FASEB journal : official publication of the Federation of
379 American Societies for Experimental Biology* 25, 66–77. 10.1096/fj.10-163147.

380 44. Vivaudou, M., Chan, K.W., Sui, J.-L., Jan, L.Y., Reuveny, E., and Logothetis, D.E. (1997).
381 Probing the G-protein Regulation of GIRK1 and GIRK4, the Two Subunits of the KACH
382 Channel, Using Functional Homomeric Mutants. *Journal of Biological Chemistry* 272,
383 31553–31560. 10.1074/jbc.272.50.31553.

384 45. Levitz, J., Broichhagen, J., Leippe, P., Konrad, D., Trauner, D., and Isacoff, E.Y. (2017).
385 Dual optical control and mechanistic insights into photoswitchable group II and III
386 metabotropic glutamate receptors. *Proc. Natl. Acad. Sci. USA* **114**, E3546–E3554.
387 10.1073/pnas.1619652114.

388